



Dielectric function and interband critical points of compressively strained ferroelectric $\text{K}_{0.85}\text{Na}_{0.15}\text{NbO}_3$ thin film with monoclinic and orthorhombic symmetry

SAUD BIN ANOOZ,^{1,*}  PETER PETRIK,^{2,3} YANKUN WANG,⁴
DESHABRATO MUKHERJEE,^{2,5} MARTIN SCHMIDBAUER,¹ AND JUTTA
SCHWARZKOPF¹

¹Leibniz-Institut für Kristallzüchtung (IKZ), Max-Born-Str. 2, 12489 Berlin, Germany

²Hungarian Research Network, Centre for Energy Research, Institute of Technical Physics and Materials Science, Budapest, Hungary

³Department of Electrical and Electronic Engineering, Institute of Physics, Faculty of Science and Technology, University of Debrecen, Hungary

⁴State Key Laboratory for Manufacturing Systems Engineering, Electronic Materials Research Laboratory, Key Laboratory of the Ministry of Education, School of Electronic Science and Engineering, Xi'an Jiaotong University, 710049 Xi'an, China

⁵Doctoral School of Materials Sciences and Technologies, Óbuda University, Budapest, Hungary

*saud.binanoz@ikz-berlin.de

Abstract: The dielectric function and interband critical points of compressively strained ferroelectric $\text{K}_{0.85}\text{Na}_{0.15}\text{NbO}_3$ thin film grown by metal-organic vapor phase epitaxy (MOVPE) are studied in broad spectral and temperature ranges by spectroscopic ellipsometry (SE). The temperature dependence of the measured pseudodielectric functions is strongly affected by a structural phase transition from the monoclinic M_c -phase to the orthorhombic c-phase at about 428 K. Using a parametric optical constant model, the corresponding dielectric functions as well as the interband optical transitions of the film are determined in the spectral range of 0.73–6.00 eV. Standard critical point (SCP) analysis of the 2nd derivatives of the dielectric functions identified three and four critical points for monoclinic and orthorhombic symmetries, respectively. A systematic redshift of the threshold energies with increasing temperatures was observed.

© 2024 Optica Publishing Group under the terms of the [Optica Open Access Publishing Agreement](#)

1. Introduction

Ferroelectric oxide materials are used in a wide spectrum of optical applications as various sensors, electro-optic modulators and infrared detectors. These materials are characterized by nonlinear optical properties, high transparency and large index of refraction in the visible spectral range [1]. Ferroelectric perovskite oxides with the chemical formula ABO_3 typically undergo a series of structural phase transitions upon cooling from the high temperature paraelectric cubic phase to various ferroelectric phases with lower crystal symmetry. Potassium sodium niobate ($\text{K},\text{Na}\text{NbO}_3$) exhibits attractive optical properties such as high transparency, high refractive index, and a large electro optic coefficient [2,3]. Being lead-free, it represents an interesting alternative for lead-based oxides in devices. Heteroepitaxially grown complex oxide films offer a number of advantages, as normally corresponding single-crystalline bulk materials cannot be easily synthesized because of their high melting points [4–7]. On the other hand, in complex oxides phase symmetry and their functional properties crucially depend on the lattice modifications induced by the epitaxial growth on lattice mismatched substrates. This concerns not only the ferroelectric polarization [6,8] but also the optical properties of the films [9,10]. Since $\text{K}_x\text{Na}_{1-x}\text{NbO}_3$ ($x \geq 0$) thin films grown under anisotropic compressive lattice strain exhibit

a monoclinic symmetry at room temperature (RT) and an orthorhombic symmetry at higher temperature [5], they represent an ideal system to investigate the influence of the phase symmetry on the dielectric function and the interband transitions. For the use of $K_xNa_{1-x}NbO_3$ thin films in optical devices a more detailed knowledge of the optical/dielectric properties of these films is necessary [11]. Spectroscopic ellipsometry (SE) is a suitable method of determining complex optical functions ($\varepsilon = \varepsilon_1 + i\varepsilon_2$) over a wide range of photon energies [4,12–15]. ε is related to the electronic band structure and electronic transitions in the material [16] and is connected to the refractive index (n) and the extinction coefficient (k) via $\varepsilon_1 = n^2 - k^2$ and $\varepsilon_2 = 2nk$.

In the present work, we apply SE to determine the optical constants in the spectral range of 0.7–6 eV of a ferroelectric $K_{0.85}Na_{0.15}NbO_3$ thin film below and above the phase transition at 428 K where the low temperature monoclinic M_c -phase transforms to the high temperature orthorhombic c -phase. The $K_{0.85}Na_{0.15}NbO_3$ thin film was grown by metal-organic vapor phase epitaxy which provides well-ordered and stoichiometric films [17,18]. The optical band gap energy is determined by using a linear extrapolation of the absorption coefficients [19,20] and revealed redshift. The energies of interband critical points (CP) are specified by using the standard critical point model [21] analysis of the 2nd derivative of the dielectric function. We identify four critical points (CP) in the M_c and c -phases between 3.5 and 6 eV. The temperature dependence of the CPs at 4.70 eV and 4.87 eV exhibits an anomaly at about 428 K, which is a signature of the phase transition. Our results underline the importance of a basic understanding of the impact of the phase symmetry on the optical properties.

2. Experimental

A $K_{0.85}Na_{0.15}NbO_3$ film with a nominal thickness of about 40 nm was grown on a 0.1° off-oriented (110) $Gd_{0.6}Sm_{0.4}ScO_3$ (GSSO) substrate by liquid-delivery spin metal-organic vapor phase epitaxy (MOVPE), for details the reader is referred to Ref. [18]. Prior to the deposition process, the $Gd_{0.6}Sm_{0.4}ScO_3$ substrate was annealed at 1373 K in pure oxygen atmosphere for 10 hours to obtain a pure ScO_2 surface termination [22]. At room temperature the $Gd_{0.6}Sm_{0.4}ScO_3$ substrate exhibits an orthorhombic symmetry. As a consequence, the (110) surface unit cell exhibits slightly different in-plane lattice parameters of 2×3.973 Å and 2×3.978 Å along the $[001]_{GSSO}$ and $[1\bar{1}0]_{GSSO}$ directions, respectively [23]. Note that the index “GSSO” refers to the $Gd_{0.6}Sm_{0.4}ScO_3$ substrate for which we use the orthorhombic notation throughout. Also bulk $(K,Nb)NbO_3$ displays an orthorhombic symmetry at room temperature, but for reasons of simplicity, we use the pseudocubic (pc) notation [24] to describe the unit cell dimensions of $K_{0.85}Na_{0.15}NbO_3$ with lattice parameters of $a_{pc} = 3.964$ Å and $b_{pc} = c_{pc} = 4.025$ Å. A comparison of the lattice parameters of $Gd_{0.6}Sm_{0.4}ScO_3$ and $K_{0.85}Na_{0.15}NbO_3$ suggests a c_{pc} surface orientation of the film, as this is expected to cause the lowest in-plane strain and thus the smallest epitaxial strain energy. In this orientation the b_{pc} axis experiences strong compressive lattice strain of −1.2% while the a_{pc} axis grows under slight tensile lattice strain of +0.2% (more details can be found in Refs. [17,25]). The surface morphology of $K_{0.85}Na_{0.15}NbO_3$ film was examined by using atomic force microscopy (AFM, Dimension Icon, Bruker). The ferroelectric domain pattern of the epitaxial film was visualized using piezoresponse force microscopy (Asylum Research, MFP-3D standalone) in a dual AC resonance tracking mode. High-resolution X-ray diffractometry (HR-XRD) was carried out on a 9 kW SmartLab system (Rigaku) using Cu $K\alpha_1$ radiation ($\lambda = 1.54056$ Å). Fast two-dimensional (2D) X-ray reciprocal space mappings (RSM) were carried out using a 2D area detector (HyPix-3000). An Anton Paar DHS 1100 heating stage enabled measurements under non-ambient conditions (in air). Ellipsometric data were collected using a Woollam M2000DI rotating compensator ellipsometer in the spectral range of 0.73–6 eV at an angle of incidence of 60°. Temperature dependent measurements were performed with a heating stage between room temperature and 523 K.

3. Results and discussion

Figure 1(a) shows a 2θ - ω HR-XRD scan in the vicinity of the symmetrical out-of-plane (110) Bragg reflection of the $\text{Gd}_{0.6}\text{Sm}_{0.4}\text{ScO}_3$ substrate. The $\text{K}_{0.85}\text{Na}_{0.15}\text{NbO}_3$ film peak appears at slightly lower 2θ values than the expected value for $(001)_{\text{pc}}$ oriented bulk $\text{K}_{0.85}\text{Na}_{0.15}\text{NbO}_3$ (marked as red dashed line). This proves $(001)_{\text{pc}}$ surface orientation of the film and net compressive in-plane strain. Pronounced thickness fringes are observed on both sides of the film peak, attesting that both film surface and film-substrate interface are smooth.

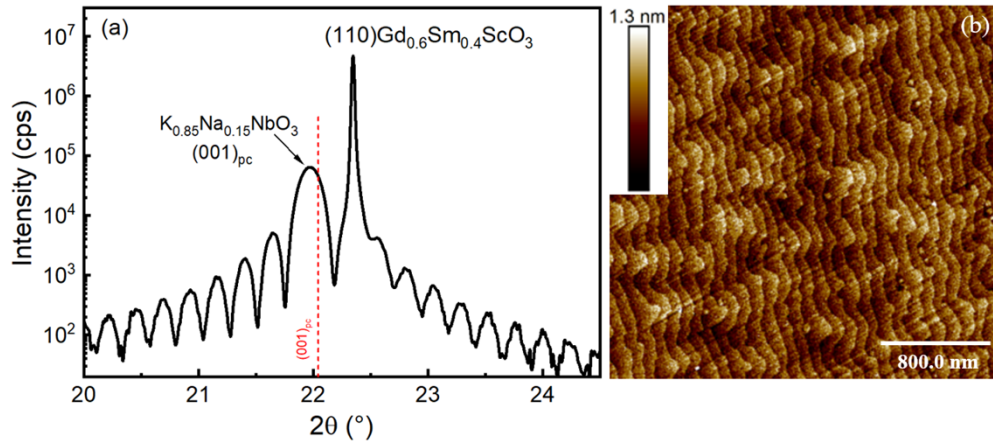


Fig. 1. (a) 2θ - ω scan of a $\text{K}_{0.85}\text{Na}_{0.15}\text{NbO}_3$ thin film in the vicinity of the (110) out-of-plane Bragg reflection of the $\text{Gd}_{0.6}\text{Sm}_{0.4}\text{ScO}_3$ substrate. The red dashed line indicates the nominal angular position of bulk $\text{K}_{0.85}\text{Na}_{0.15}\text{NbO}_3$ with $(001)_{\text{pc}}$ surface orientation. (b) Corresponding atomic force micrograph of the film surface.

From the angular period of the intensity fringes a film thickness of (39 ± 1) nm can be deduced. The AFM image in Fig. 1(b) confirms the smooth surface of the $\text{K}_{0.85}\text{Na}_{0.15}\text{NbO}_3$ film. The surface morphology mimics the step-and-terrace structure of the substrate prior to growth due to the 0.1° off-orientation, i.e., it is formed of regularly spaced surface steps, indicating a step-flow growth mode with a very low root mean square (rms) surface roughness of about 0.15 nm. To investigate the phase transition from the monoclinic M_c -phase to the orthorhombic c -phase in the epitaxial $\text{K}_{0.85}\text{Na}_{0.15}\text{NbO}_3$ film, temperature dependent X-ray reciprocal space mappings and corresponding lateral PFM measurements were performed. Figures 2(a)-(d) show lateral PFM micrographs (amplitude images) when the temperature is increased from 300 K to 433 K.

At 300 K (Fig. 2(a)) a very regular periodic stripe domain pattern typical for M_c domains [5] is observed, which is still preserved at 363 K (Fig. 2(b)). When further increasing the temperature to 423 K (Fig. 2(c)) the periodicity of the domain pattern shows clear disturbances and finally disappears completely at 433 K (Fig. 2(d)). In Figs. 2(e)-(h) the corresponding X-ray reciprocal space maps in the vicinity of the asymmetric $(444)_{\text{GSSO}}$ substrate Bragg reflection (containing both in-plane and out-of-plane scattering vector components) are presented. At 300 K (Fig. 2(e)) a complex diffraction pattern including strong and equally spaced satellite reflections is observed which is caused by the periodic arrangement of the monoclinic M_c -domains [5]. When increasing the temperature, the satellite pattern starts to be less prominent, indicating a reduction of the regularity of the domain pattern, which is in accordance with the corresponding PFM images. Between 423 K (Fig. 2 g) and 433 K (Fig. 2 h) the satellite pattern has completely vanished confirming the absence of a periodic domain structure, again in agreement with the PFM images shown in Fig. 2(c,d).

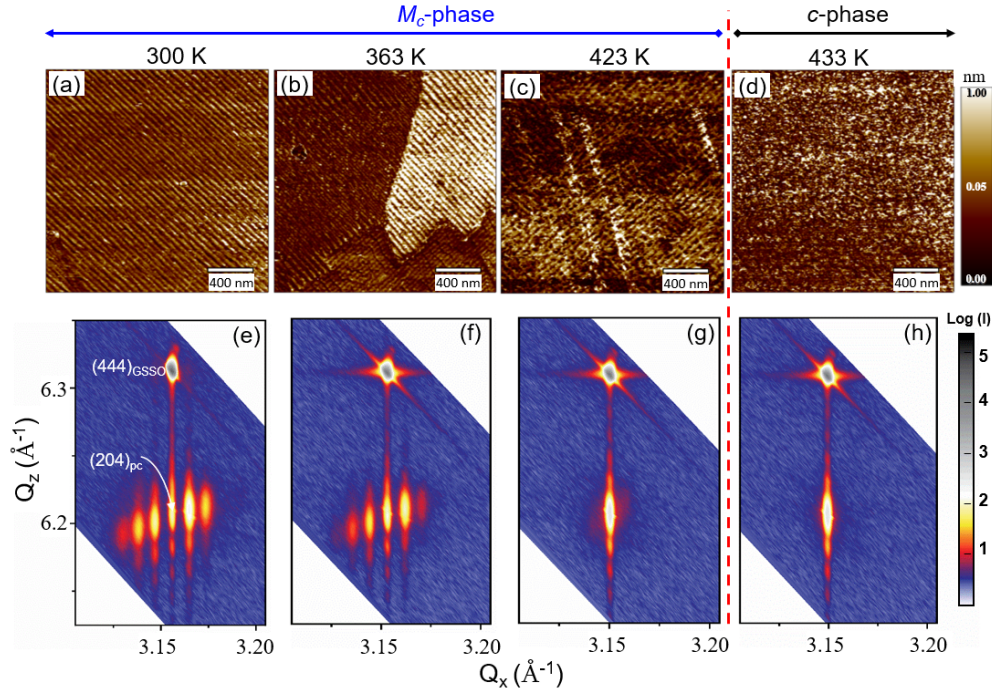


Fig. 2. (a-d) Lateral piezoresponse force micrographs (amplitude images) of the $\text{K}_{0.85}\text{Na}_{0.15}\text{NbO}_3$ strained film grown on (110) $\text{Gd}_{0.6}\text{Sm}_{0.4}\text{ScO}_3$ substrate recorded at different temperatures, (e-h) corresponding X-ray reciprocal space maps in the vicinity of the sharp $(444)_{\text{GSSO}}$ substrate Bragg reflection.

In accordance with our previous results [5], this implies the absence of a monoclinic distortion, and instead points to an orthorhombic symmetry of the $\text{K}_{0.85}\text{Na}_{0.15}\text{NbO}_3$ unit cells. Meanwhile, the center position of the X-ray intensity scattered by the film is still at the same horizontal $Q_x = Q_{001}$ position as the $(444)_{\text{GSSO}}$ substrate Bragg reflection proving that the film does not undergo any plastic lattice relaxation but perfectly preserves its fully strained relation to the substrate. Note that the (110) oriented $\text{Gd}_{0.6}\text{Sm}_{0.4}\text{ScO}_3$ substrate exhibits a non-squared surface unit cell, so that a tetragonal symmetry is not possible in the clamped layer. More details on this issue can be found elsewhere [5,6,8,18,26,27]. In summary, from Fig. 2 we conclude a structural phase transition from a monoclinic M_c -phase to an orthorhombic c-phase between 423 K and 433 K.

In order to evaluate the optical properties, ellipsometric measurements in the energy range of 0.73–6.0 eV were performed. The complex reflectance ratio of the light polarized parallel and perpendicular to the plane of incidence (R_p and R_s , respectively) was measured and can be expressed by [12]:

$$\frac{R_p}{R_s} = \tan(\psi) \cdot e^{i\Delta}, \quad (1)$$

where $\tan(\psi)$ is the amplitude ratio and Δ the phase difference. The reflection coefficients R_p and R_s are related to physical characteristics of the sample, such as refractive index (n) and extinction coefficient (k), through Fresnel equations [28]. To evaluate the temperature dependence of the optical properties of the film we determined the pseudodielectric function $\langle \epsilon \rangle = \langle \epsilon_1 \rangle + i \langle \epsilon_2 \rangle$ (see for more details in Supplement 1) by the measurement of the ellipsometric angles ψ and Δ under continuous heating and cooling at 3.5 eV. Since the energy of 3.5 eV is close to the optical absorption edge the pseudodielectric function is sensitive to structural changes that occur

during a phase transition [29,30]. The real and imaginary parts of the pseudodielectric function $\langle \varepsilon_1 \rangle$ and $\langle \varepsilon_2 \rangle$ of the $\text{K}_{0.85}\text{Na}_{0.15}\text{NbO}_3$ film are plotted in Figs. 3(a) and (b), respectively. They show a strong increase as well as a respective decrease in the temperature range between 300 K and 523 K and pronounced discontinuity at the phase transition temperature (~ 428 K). This behavior is essentially attributed to the $\text{K}_{0.85}\text{Na}_{0.15}\text{NbO}_3$ thin film, since $\langle \varepsilon_1 \rangle$ and $\langle \varepsilon_2 \rangle$ of a bare $\text{Gd}_{0.6}\text{Sm}_{0.4}\text{ScO}_3$ substrate do not exhibit any significant changes in this temperature range, but basically show constant values (corresponding data are additionally shown in Fig. 3(a) and (b) as blue triangles). To extract the optical constants from the SE measurements, we used a model, which consists of a four-component stack composed of air/surface roughness/film/ substrate, to fit ψ and Δ . The quality of such fit is described by the mean squared error (MSE), representing the difference between measured and modeled data [31].

$$MSE = \sqrt{\frac{1}{2n - m} \sum_{i=1}^n \left[(\psi_{exp} - \psi_{mod})^2 + (\Delta_{exp} - \Delta_{mod})^2 \right]} \times 1000 \quad (2)$$

where n is the number of (ψ, Δ) pairs, m is the number of fit parameters, and *exp* and *mod* refer to experimentally measured data and theoretically modeled data, respectively. For the surface roughness layer we used the Bruggeman effective medium approximation [32] with a [50% bulk film]/[50% void] mixture.

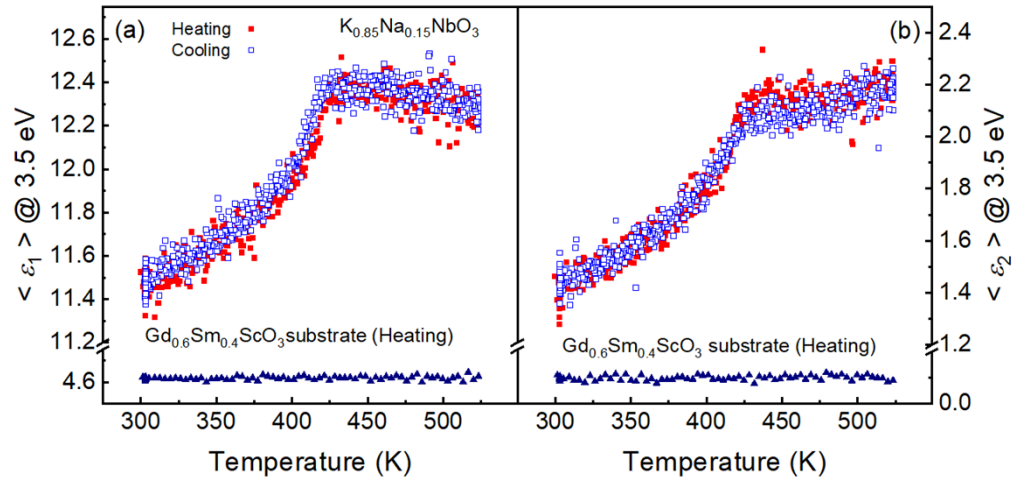


Fig. 3. Temperature dependent spectra of the real (a) and imaginary (b) parts of the pseudodielectric function of the $\text{K}_{0.85}\text{Na}_{0.15}\text{NbO}_3$ film and the $\text{Gd}_{0.6}\text{Sm}_{0.4}\text{ScO}_3$ substrate determined at 3.5 eV.

We would like to point out that we treat the optical properties as isotropic. This approach is justified since the off-diagonal elements of the Müller matrix are nearly zero in the entire spectral range (see Supplement 1, Fig. S1a and b). Furthermore, rotating the sample from 0° to 360° in 10° -steps revealed that the Jones matrix elements [13] vanish for measurements along $[001]_{\text{GSSO}}$ (corresponds to rotation angle 0°) and $[1\bar{1}0]_{\text{GSSO}}$ directions (corresponds to rotation angle 90° , see Supplement 1, Fig. S1c). On the other hand, the very weak influence of a preferred domain orientation (Fig. 2) on the in-plane anisotropic dielectric function can be explained by the fact that the size of the light spot on the sample (about 1 mm) is much larger than the lateral dimensions of the ferroelectric domains. Therefore, all measurements were carried out exclusively along the $[001]_{\text{GSSO}}$ in-plane direction.

First, we determined the film thickness based on our model described above and the Sellmeier equation to describe the dispersion relation of the refractive index n [33]. By considering/examining only the absorption-free spectral range (< 3 eV) at room temperature, where the

light is coherently reflected by the substrate, we obtained a film thickness and surface roughness of (38.4 ± 0.2) nm and (0.84 ± 0.02) nm, respectively. The film thickness is in good agreement with the X-ray data (39 ± 1) nm while the surface roughness is slightly overestimated compared to the AFM rms surface roughness of 0.15 nm. Despite the deviation in the surface roughness (which can be attributed to the specific measurements conditions and evaluation of AFM and SE data [34,35], the result basically confirms our model assumption.

The approach in this study is to obtain a mathematical and Kramers-Kronig consistent determination of the dielectric function by means of B-splines [36,37] (see the Supplement 1). Such a treatment of the deposited $\text{K}_{0.85}\text{Na}_{0.15}\text{NbO}_3$ film requires no prior knowledge about the film properties or assumptions about the interaction of light with the film. B-splines have already proven their effectiveness for material modeling in multiple spectroscopic ellipsometry applications [36–39]. The dielectric function (ϵ) of $\text{K}_{0.85}\text{Na}_{0.15}\text{NbO}_3$ layer was constructed by the B-spline formula [36]. A spline function is basically a series of polynomial segments, which is constructed in a manner to maintain continuity up to a certain degree of differentiation. On the other hand, the Kramers-Kronig (K-K) integral can be applied to the B-spline recursion formula to generate K-K consistent basis functions (i.e., the ϵ_1 curve is defined by the K-K transformation of ϵ_2) [36,39]. However, there is a problem that arises from the number of knots (resolution) used to describe the dielectric function. Using fewer knots in the considered wavelength range can lead to data underfitting and some relevant spectral features will be neglected. On the other hand, if there are too many knots within the wavelength range beyond the optimal value there is a risk of overfitting the data and, hence, to catch random noise in the data or unrealistic curve bending [40]. To solve this problem different resolutions were used to optimally fit the experimental data using B-splines. The resolution of 0.2 eV implemented in this study was the best one in terms of consistent optical constants, which was verified by the comparison with analytical models of physical relevance (Gaussian dispersion) (see Fig S2 in the Supplement 1). Polynomial B-spline functions [36,39] (see the Supplement 1) are used to fit the measured SE angles ψ and Δ (MSE = 1.2) for the entire photon energy range (0.73–6.0 eV) recorded at room temperature, where the film is in the M_c -phase, and at 523 K, well above the phase transition to the c -phase; both experimental and simulation data of the ellipsometry angles ψ and Δ for the M_c -phase (black squares) and the c -phase (red circles) are presented in Fig. 4(a).

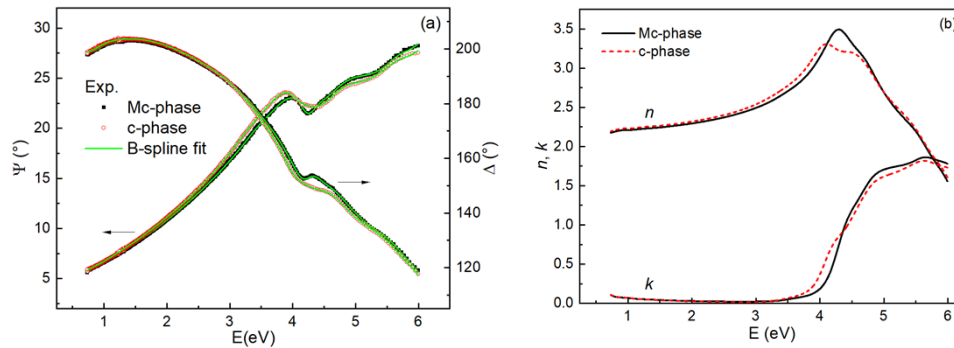


Fig. 4. (a). Ellipsometric angles Ψ and Δ measured for the M_c phase at room temperature and the c -phase at 523 K as well as results from fitting with B-spline functions (green lines) as a function of the photon energy, (b) Refractive index n and extinction coefficient k as a function of photon energy in the M_c -phase (black curves) and c -phase (red dotted lines) for the epitaxial $\text{K}_{0.85}\text{Na}_{0.15}\text{NbO}_3$ film on $\text{Gd}_{0.6}\text{Sm}_{0.4}\text{ScO}_3$ substrate.

From the B-spline fit, the refractive index (n) and the extinction coefficient (k) are calculated as a function of the energy and shown in Fig. 4(b) for the M_c phase (black lines) and the c -phase

(red lines). While in the energy range up to ~ 3.5 eV the extinction coefficient k is close to zero indicating a transparent region, the refractive index n slightly increases from 2.2 to about 2.5 for both phases. A strong increase in k displays the onset of absorption at higher energies, which also results in an increase of n until a maximum is obtained at ~ 4.5 eV and subsequently a strong decrease, often observed for many perovskite oxide thin films [9,41]. From Fig. 4(b) we also conclude that n and k are quite similar for the film in the monoclinic M_c -phase and the orthorhombic c-phase in the transparent region, but in the absorption region (> 3.5 eV) significant differences can be detected.

For a more detailed analysis, the absorption coefficient (α) of the $K_{0.85}Na_{0.15}NbO_3$ film is calculated in the energy range between 0.73 eV and 6.0 eV by $\alpha = 4\pi k/\lambda$, where λ is the wavelength of the incident light and k is the extinction coefficient. The optical band gaps are deduced from Tauc plots [19], where the low energy part of the measured absorption coefficient is fitted with a power function $(\alpha E) = (E - E_g)^r$ [20]. The exponent r depends on the nature of the transition with $r = 0.5$ and 2 for direct and indirect allowed transitions, respectively. For $K_{0.85}Na_{0.15}NbO_3$, the valence band is primarily constituted by the O 2p states, while the conduction band derives from the transition-metal (Nb) d orbitals. The d band consists of a lower energy, wide $d\epsilon$ sub-band and a higher energy, narrower $d\gamma$ sub-band [42,43]. On the basis of density functional theory calculations [44,45] and experimental data [42] for (K,Na)NbO₃ we assume an indirect band gap. By extrapolating the linear fit using $(\alpha E)^{1/2} = (E - E_g)$ we determined the indirect band gaps to be (3.75 ± 0.02) eV and (3.60 ± 0.02) eV at room temperature (M_c -phase) and 523 K (c-phase), respectively, indicating a significant redshift. The redshift of the absorption edge is due to temperature-dependent dilatation of the lattice, while the main contribution comes from the electron-lattice interaction [46]. Chernova et al. [9] reported a bandgap energy of 3.53 eV in a $K_{0.5}Na_{0.5}NbO_3$ film on SrTiO₃ substrate. The large value of the band gap (3.75 ± 0.02) eV of $K_{0.85}Na_{0.15}NbO_3$ is tentatively explained by the ferroelectric polarization induced by compressive lattice strain, which leads to additional bandgap widening [47,48].

The temperature dependence of the real (ϵ_1) and imaginary (ϵ_2) parts of the dielectric function in the photon energy range of 2 - 6 eV is presented in Fig. 5. Several (local) maxima and minima in the dielectric function (3.8 - 6 eV) can be observed.

For example, the real part of the dielectric function clearly shows the occurrence of a new maximum at about 4.5 eV (435 K) in the c-phase. These local extrema are typically referred to as critical points (CP) [49] and are related to electronic interband transitions from the highest valence bands to the lowest conduction bands at various regions in the Brillouin zone [50]. In order to investigate this in more detail, we have evaluated the real and imaginary parts of the dielectric function of the $K_{0.85}Na_{0.15}NbO_3$ thin film only in the absorption region (> 3 eV) at 300 K (M_c -phase) and 523 K (c-phase) (Fig. 6(a)).

A standard critical point (SCP) analysis of the 2nd derivatives $d^2\epsilon/dE^2$ of the dielectric function was performed to identify interband transitions by:

$$\frac{d^2\epsilon}{dE^2} = \begin{cases} t(t-1)A_m e^{i\phi_m} (E - E_m + i\Gamma_m)^{t-2}, & t \neq 0 \\ A_m e^{i\phi_m} (E - E_m + i\Gamma_m)^{-2}, & t = 0 \end{cases} \quad (3)$$

Here, A_m , E_m , Γ_m and ϕ_m are the amplitude, threshold energy, broadening, and excitonic phase angle, respectively, for the m^{th} electronic transitions [39]. The exponent t may take values of $-\frac{1}{2}$, 0, $\frac{1}{2}$ and -1 for, one-, two-, three-dimensional and excitonic lineshapes, respectively. For the evaluation of our data we choose $t = -1$ for both M_c -phase and c-phase, in accordance with previously published data for PbTiO₃ and PbZrO₃ materials [51] and based on strong excitonic interactions in perovskite oxides. The second derivatives of both the real and imaginary parts of the dielectric function of the $K_{0.85}Na_{0.15}NbO_3$ thin film were fitted with the same set of parameters.

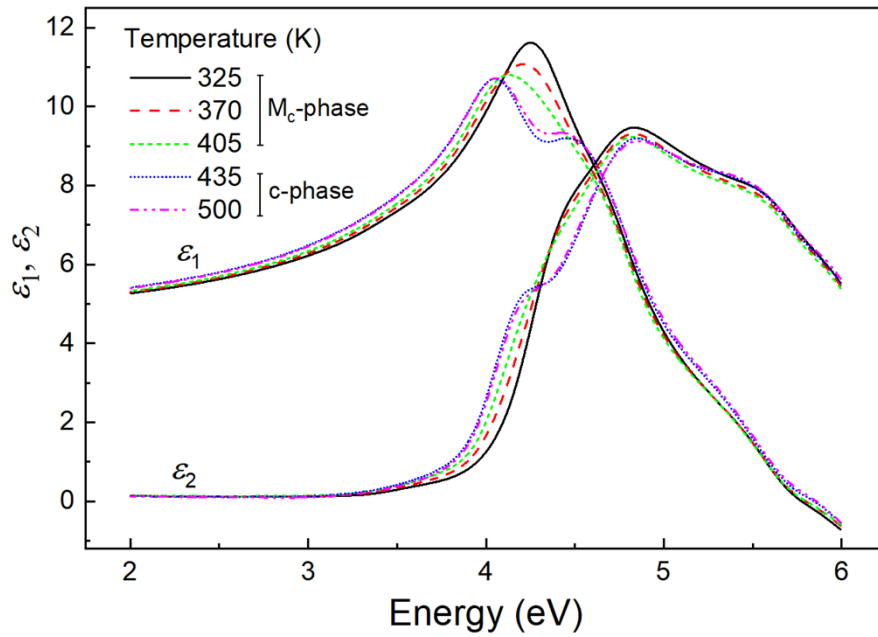


Fig. 5. Real (ϵ_1) and imaginary (ϵ_2) parts of the dielectric function at 325, 370, 405, 435 and 500 K as a function of photon energy in the epitaxial $\text{K}_{0.85}\text{Na}_{0.15}\text{NbO}_3$.

To fit the data for the M_c phase in the energy range between 3.5 and 5.75 eV, it was sufficient to superimpose three separate line profiles, each of which can be assigned to a specific critical point (CP). The corresponding energy positions are indicated by the black lines and labeled as E_a , E_b , and E_c in the order of increasing photon energy (Fig. 6(b)). However, for the c-phase (Fig. 6(c)) four critical points with corresponding energies E_a , E_b , E_N and E_c were needed to obtain good agreement between experiment and simulated curves.

The observed CPs are tentatively attributed to charge transfer transitions from O (p) to Nb (d- t_2 g) [52], and corresponding energies for the M_c -phase and the c-phase are given in Table 1.

Table 1. SCP model parameters for $\text{K}_{0.85}\text{Na}_{0.15}\text{NbO}_3$ film extracted from the best fitting of the second derivatives of the dielectric functions (Figs. 6(b) and (c)) at room temperature (M_c -phase) and 523 K (c-phase)

Ferroelectric phase		E_a	E_b	E_N	E_c
M_c	E_m (eV)	4.30 ± 0.02	4.68 ± 0.02		5.61 ± 0.02
	A_m	1.90 ± 0.01	1.49 ± 0.01		0.48 ± 0.01
	ϕ_m (°)	118 ± 2.00	90.0 ± 2.00		198 ± 2.00
	Γ_m (eV)	0.31 ± 0.01	0.36 ± 0.01		0.34 ± 0.01
c	E_m (eV)	4.10 ± 0.02	4.51 ± 0.02	4.61 ± 0.02	5.55 ± 0.02
	A_m	1.18 ± 0.01	1.33 ± 0.01	0.25 ± 0.01	0.73 ± 0.01
	ϕ_m (°)	114 ± 2.00	83.0 ± 2.00	99.6 ± 2.00	215 ± 2.00
	Γ_m (eV)	0.28 ± 0.01	0.34 ± 0.01	0.26 ± 0.01	0.41 ± 0.01

In order to investigate the critical points in more detail, we plotted the values for the threshold energies E_a , E_b , E_N and E_c as a function of the temperature in Fig. 7. With increasing temperature, a redshift of all CP energies can be observed, which is caused by temperature-dependent electron-phonon interaction [46]. For a closer look, the temperature-dependence of electronic transitions

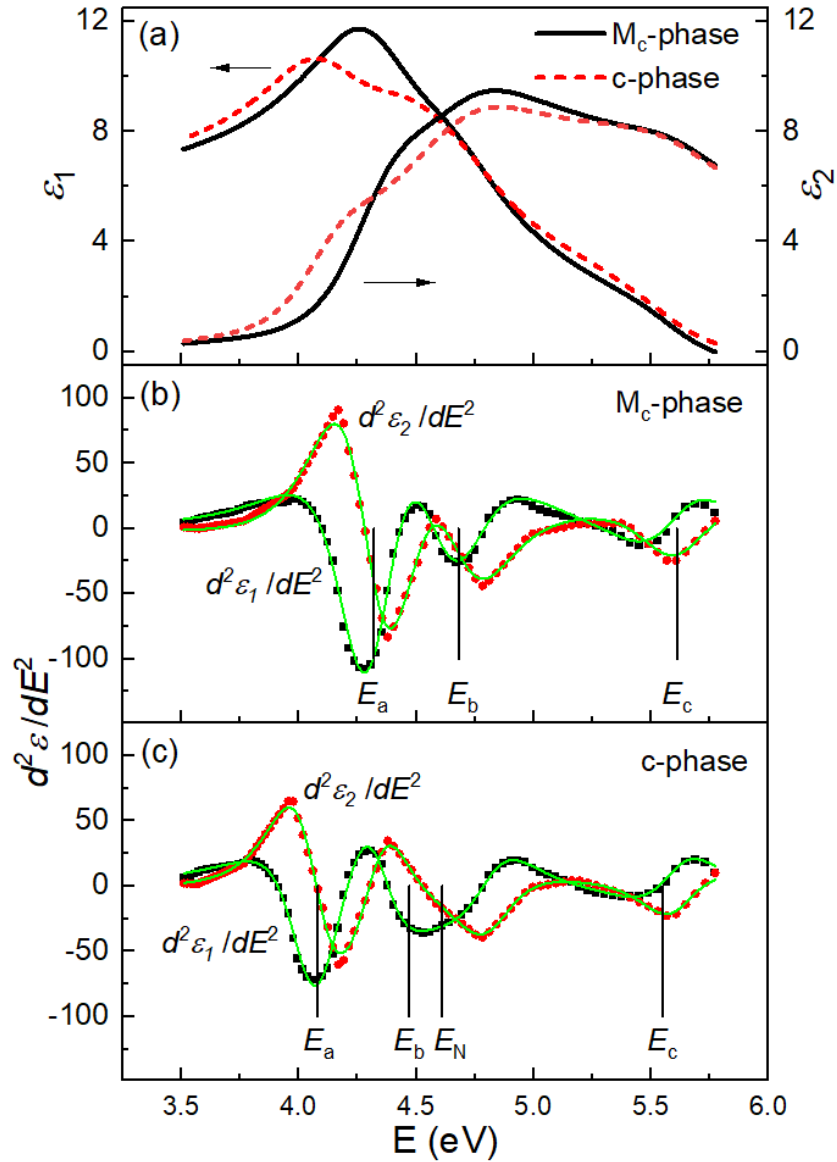


Fig. 6. (a) Real (ϵ_1) and imaginary (ϵ_2) parts of the dielectric function as a function of photon energy in the M_c -phase and c-phase. Experimental (dots) and the best-fit (solid lines) data for the second derivatives of ϵ_1 and ϵ_2 in the (b) M_c -phase and (c) c-phase, respectively, of the $K_{0.85}Na_{0.15}NbO_3$ film. The vertical blue lines indicate four interband electronic transitions.

was fitted independently for the M_c and c-phases using a linear function $E(T) = E_0 - \beta T$, with E_0 is the transition energy at 0 K and β the temperature coefficient.

The resulting temperature coefficients of E_a , E_b , E_N and E_c are presented in Table 2. Figure 7 reveals that in the range of the phase transition, the threshold energies E_a , E_b and E_c show a clear discontinuity. Furthermore, the phases below (M_c) and above (c) the phase transition temperature have different temperature coefficients which are always larger in the monoclinic M_c phase than in the orthorhombic c-phase. The values in the range of 10^{-4} eV/K are in good agreement

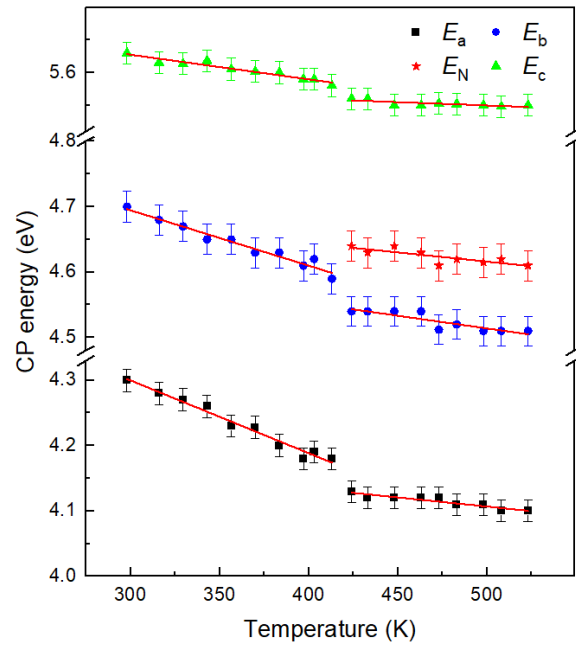


Fig. 7. Temperature dependence of the threshold energies E_a , E_b , E_N and E_c .

with temperature coefficients for Pb-oxide based ferroelectric materials [16,53]. The significant decrease in the transition region has similarly been observed for $\text{Pb}(\text{Zr,Ti})\text{O}_3$ -related materials [53] and $\text{Na}_{0.5}\text{Bi}_{2.5}\text{Nb}_{2-x}\text{W}_x\text{O}_{9+\delta}$ ferroelectric ceramics [54] in the phase transition region.

Table 2. Temperature coefficients of E_a , E_b , E_N and E_c in the M_c - and c -phases.

Critical points	Temperature coefficient, β (eV/K)	
	M_c -phase	c -phase
E_a	$(9.00.2) \times 10^{-4}$	$(4.00.2) \times 10^{-4}$
E_b	$(8.50.2) \times 10^{-4}$	$(3.80.2) \times 10^{-4}$
E_N		$(2.80.2) \times 10^{-4}$
E_c	$(3.70.2) \times 10^{-4}$	$(1.00.2) \times 10^{-4}$

Our results indicate that electronic transitions are very sensitive to structural variations during the transition from the M_c -phase (monoclinic) to the c -phase (orthorhombic) and the narrow temperature range where both phases coexist. Moreover, we observe an additional transition E_N near 4.67 eV (425 K) in the orthorhombic c -phase (Fig. 7), which does not exist in the monoclinic M_c -phase.

On first sight, the experimentally observed strong phase dependence is not expected since former calculations [55–57] on KNbO_3 bulk crystals have shown that similar band structures emerge for the cubic paraelectric phase as well as for the tetragonal, orthorhombic and rhombohedral phases. Schmidt et al [43], reported that in all phases of KNbO_3 including the orthorhombic and monoclinic ones, there are states elsewhere in the Brillouin zone which are nearly degenerate with the valence band maximum or the conduction band minimum. Such near-degeneracies strongly influence the optical properties because the electronic transitions at different k -points are strongly mixed in the optical response. However, differences between bulk crystals and

strained epitaxial films have been demonstrated [58–60]. Tyunina et al. [58] demonstrated, that epitaxy of strained thin films causes dramatic changes of the interband transitions compared to a reference KNbO_3 crystal: the energies of transitions change, some transitions are significantly suppressed while new transitions also appear. Corresponding first-principle calculations on the monoclinic and orthorhombic phases (among others) in strained NaNbO_3 films have also shown differences in the band structure [61]. To shed light on the variation of the CP energies, the microstructure has to be considered. The ABO_3 perovskite structure is a three-dimensional network of regular corner-linked BO_6 octahedra with small B cations in the center of each octahedron [55]. Li et al. [45] reported that the Nb-O bond lengths change, and the angles of O-Nb-O bonds deviate from 90° when the crystal symmetry of NaNbO_3 changes. Li et al. [54] attributed the appearance of an additional transition for the $\text{Na}_{0.5}\text{Bi}_{2.5}\text{Nb}_{2-x}\text{W}_x\text{O}_{9+\delta}$ ferroelectric material to the structural distortion induced by the phase transition. Here we speculate that the transformation from the monoclinic (M_c) to the orthorhombic phase (c -phase) shifts the Nb position of the NbO_6 octahedron [62]. This affects the orbital hybridization and leads to appearance of new electronic transition. Similarly, Zhang et al. [63] reported the emergence of an additional electronic transition upon the phase transition from the tetragonal to the cubic phase in $0.93\text{Pb}(\text{Zn}_{1/3}\text{Nb}_{2/3})\text{O}_3$ - 0.07PbTiO_3 single crystals which could be attributed to a transition from the O 2p to the conducting Nb- $4d_{xz}$ state.

4. Conclusion

Spectroscopic ellipsometry was used to reveal the dielectric functions for a compressively strained $\text{K}_{0.85}\text{Na}_{0.15}\text{NbO}_3$ film at room temperature for the monoclinic M_c -phase and above the phase transition in the orthorhombic c -phase at 523 K c -phase. The dielectric functions showed significant differences in the spectral region above 3.5 eV. By using standard critical point model analysis, we identify three and four critical points energy in the M_c and c -phases, respectively. A redshift of the critical points and additional absorption peak with increasing temperature was observed. Temperature-dependent analysis of the threshold energies of the critical points E_a , E_b , and E_c revealed clearly different behavior in the monoclinic and orthorhombic phase, with considerably higher temperature coefficient for the M_c -phase as compared to that of the c -phase.

Funding. HUN-REN Hungarian Research Network Cloud project (C1792954); Hungarian National Science Fund (K146181, TKP 2021-EGA04); European Regional Development Fund (I.8/15).

Acknowledgments. The (Gd,Sm)ScO₃ substrates were grown at the Leibniz-Institut für Kristallzüchtung in the group of S. Ganschow.

Disclosures. The authors declare no conflicts of interest.

Data availability. Data underlying the results presented in this paper are not publicly available at this time but may be obtained from the authors upon reasonable request.

Supplemental document. See [Supplement 1](#) for supporting content.

References

1. B. W. Wessels, "Ferroelectric oxide epitaxial thin films: synthesis and non-linear optical properties," *J. Cryst. Growth* **195**(1-4), 706–710 (1998).
2. J. Wu, D. Xiao, and J. Zhu, "Potassium-sodium niobate lead-free piezoelectric materials: past, present, and future of phase boundaries," *Chem. Rev.* **115**(7), 2559–2595 (2015).
3. S. Sharma, V. Gupta, and M. Tomar, "Optical properties of lead-free ferroelectric potassium sodium niobate ($\text{K}_x\text{Na}_{1-x}\text{NbO}_3$) thin films," *Mater. Today: Proc.* **17**, 34–40 (2019).
4. S. Bin Anooz, Y. Wang, P. Petrik, *et al.*, "High temperature phase transitions in NaNbO_3 epitaxial films grown under tensile lattice strain," *Appl. Phys. Lett.* **120**(20), 202901 (2022).
5. L. von Helden, L. Bogula, P. E. Janolin, *et al.*, "Huge impact of compressive strain on phase transition temperatures in epitaxial ferroelectric $\text{K}_x\text{Na}_{1-x}\text{NbO}_3$ thin films," *Appl. Phys. Lett.* **114**(23), 232905 (2019).
6. J. Schwarzkopf, D. Braun, M. Hanke, *et al.*, "Strain Engineering of Ferroelectric Domains in $\text{K}_x\text{Na}_{1-x}\text{NbO}_3$ Epitaxial Layers," *Front. Mater.* **4**, 26 (2017).
7. R. Xu, J. Huang, E. S. Barnard, *et al.*, "Strain-induced room-temperature ferroelectricity in SrTiO_3 membranes," *Nat. Commun.* **11**(1), 3141 (2020).

8. M. Schmidbauer, M. Hanke, A. Kwasniewski, *et al.*, “Scanning X-ray nanodiffraction from ferroelectric domains in strained $\text{K}_{0.75}\text{Na}_{0.25}\text{NbO}_3$ epitaxial films grown on (110) TbScO_3 ,” *J. Appl. Crystallogr.* **50**(2), 519–524 (2017).
9. E. Chernova, O. Pacheroova, T. Kocourek, *et al.*, “Optical Properties of Ferroelectric Epitaxial $\text{K}_{0.5}\text{Na}_{0.5}\text{NbO}_3$ Films in Visible to Ultraviolet Range,” *PLoS One* **11**(4), e0153261 (2016).
10. C. Teply, B. A. Tyler, and R. F. Berger, “Tuning the Band Gaps of Oxide and Halide Perovskite Compounds via Biaxial Strain in All Directions,” *J. Phys. Chem. C* **125**(47), 25951–25958 (2021).
11. I. Vurgaftman, J. R. Meyer, and L. R. Ram-Mohan, “Band parameters for III–V compound semiconductors and their alloys,” *J. Appl. Phys.* **89**(11), 5815–5875 (2001).
12. R. M. A. Azzam and N. M. Bashara, *Ellipsometry and Polarized Light* (North-Holland, Amsterdam, 1977).
13. H. Fujiwara, 2007, “*Spectroscopic Ellipsometry: Principles and Applications*,” (New York: Wiley).
14. G. E. Jellison and F. A. Modine, “Parameterization of the optical functions of amorphous materials in the interband region,” *Appl. Phys. Lett.* **69**(3), 371–373 (1996).
15. S. Bin Anooz, J. Schwarzkopf, R. Dirsyte, *et al.*, “Spectroscopic ellipsometry studies on the optical constants of $\text{Bi}_4\text{Ti}_3\text{O}_{12}:\text{xNa}$ thin films grown by metal-organic chemical vapor deposition,” *Thin Solid Films* **519**(11), 3782–3788 (2011).
16. Z. H. Duan, Z. G. Hu, K. Jiang, *et al.*, “Temperature-dependent dielectric functions and interband critical points of relaxor lead hafnate-modified $\text{PbSc}_{1/2}\text{Ta}_{1/2}\text{O}_3$ ferroelectric ceramics by spectroscopic ellipsometry,” *Appl. Phys. Lett.* **102**(15), 151908 (2013).
17. J. Schwarzkopf, D. Braun, M. Hanke, *et al.*, “Monoclinic MA domains in anisotropically strained ferroelectric $\text{K}_{0.75}\text{Na}_{0.25}\text{NbO}_3$ films on (110) TbScO_3 grown by MOCVD,” *J. Appl. Crystallogr.* **49**(2), 375–384 (2016).
18. Y. Wang, S. Bin Anooz, G. Niu, *et al.*, “Thickness effect on ferroelectric domain formation in compressively strained $\text{K}_{0.65}\text{Na}_{0.35}\text{NbO}_3$ epitaxial films,” *Phys. Rev. Mater.* **6**(8), 084413 (2022).
19. J. Tauc, R. Grigorovici, and A. Vancu, “Optical Properties and Electronic Structure of Amorphous Germanium,” *Phys. Status Solidi B* **15**(2), 627–637 (1966).
20. J. I. Pankov, *Optical Processes in Semiconductors*, (Dover, 1975), Chap. 3.
21. M. Cardona, in *Modulation Spectroscopy, Suppl. 11 of Solid State Physics*, edited by F. Seitz, D. Turnbull, and H. Ehrenreich, eds. (Academic, New York, 1969).
22. J. E. Kleibecker, B. Kuiper, S. Harkema, *et al.*, “Structure of singly terminated polar DyScO_3 (110) surfaces,” *Phys. Rev. B* **85**(16), 165413 (2012).
23. R. Uecker, D. Klimm, R. Bertram, *et al.*, “Growth and Investigation of $\text{Nd}_{1-x}\text{Sm}_x\text{ScO}_3$ and $\text{Sm}_{1-x}\text{Gd}_x\text{ScO}_3$ Solid-Solution Single Crystals,” *Acta Phys. Pol. A* **124**(2), 295–300 (2013).
24. A. Vailionis, H. Boschker, W. Siemons, *et al.*, “Misfit strain accommodation in epitaxial ABO_3 perovskites: Lattice rotations and lattice modulations,” *Phys. Rev. B* **83**(6), 064101 (2011).
25. J. Schwarzkopf, D. Braun, M. Schmidbauer, *et al.*, “Ferroelectric domain structure of anisotropically strained NaNbO_3 epitaxial thin films,” *J. Appl. Phys.* **115**(20), 204105 (2014).
26. M. Schmidbauer, L. Bogula, B. Wang, *et al.*, “Temperature dependence of three-dimensional domain wall arrangement in ferroelectric $\text{K}_{0.9}\text{Na}_{0.1}\text{NbO}_3$ epitaxial thin films,” *J. Appl. Phys.* **128**(18), 184101 (2020).
27. P. Gaal, D. Schmidt, M. Khosla, *et al.*, “Self-stabilization of the equilibrium state in ferroelectric thin films,” *Appl. Surf. Sci.* **613**, 155891 (2023).
28. E. Hecht, eds. (2002), “*Optics*,” 4th ed., Reading, (MA: Addison–Wesley).
29. I. Aulika, A. Dejneka, A. Lynnyk, *et al.*, “Thermo-optical investigations of NaNbO_3 thin films by spectral ellipsometry,” *Phys. Status Solidi (c)* **6**(12), 2765–2768 (2009).
30. Y. F. Tsay, B. Bendow, and S. S. Mitra, “Theory of the Temperature Derivative of the Refractive Index in Transparent Crystals,” *Phys. Rev. B* **8**(6), 2688–2696 (1973).
31. J. A. Woollam Co., Inc., “Guide to using WVASE32: software for spectroscopic ellipsometry data acquisition and analysis,” Lincoln, NE, USA (1995).
32. D. Bruggeman, “Berechnung verschiedener physikalischer Konstanten von heterogenen Substanzen,” *Ann. Phys. (Berlin, Ger.)* **416**, 636–664 (1935).
33. H. Fujiwara, R. Collins, J. Hilfiker, *et al.*, “Chapter 5: Dielectric Function Modeling,” *Spectroscopic Ellipsometry for Photovoltaics Volume 1: Fundamental Principles and Solar Cell Characterization* **1**, pgs 115–153 (2018).
34. P. Petrik, L. P. Biró, M. Fried, *et al.*, “Comparative study of surface roughness measured on polysilicon using spectroscopic ellipsometry and atomic force microscopy,” *Thin Solid Films* **315**(1–2), 186–191 (1998).
35. B. Fodor, P. Kozma, S. Burger, *et al.*, “Effective medium approximation of ellipsometric response from random surface roughness simulated by finite-element method,” *Thin Solid Films* **617**, 20–24 (2016).
36. B. Johs and J. S. Hale, “Dielectric function representation by B-splines,” *Physica Status Solidi (a)* **205**(4), 715–719 (2008).
37. J. W. Weber, T. A. R. Hansen, M. C. M. van de Sanden, *et al.*, “B-spline parametrization of the dielectric function applied to spectroscopic ellipsometry on amorphous carbon,” *J. Appl. Phys.* **106**(12), 123503 (2009).
38. S. G. Choi, H. Y. Zhao, C. Persson, *et al.*, “Dielectric function spectra and critical-point energies of $\text{Cu}_2\text{ZnSnSe}_4$ from 0.5 to 9.0 eV,” *J. Appl. Phys.* **111**(3), 033506 (2012).
39. D. V. Likhachev, “Certain topics in ellipsometric data modeling with splines: a review of recent developments,” *Adv. Opt. Technol.* **11**(3–4), 93–115 (2022).

40. D. V. Likhachev, "Spectroscopic ellipsometry data analysis using penalized splines representation for the dielectric function," *Thin Solid Films* **669**, 174–180 (2019).
41. S. Bin Anooz, P. Petrik, M. Schmidbauer, *et al.*, "Refractive index and interband transitions in strain modified NaNbO_3 thin films grown by MOCVD," *J. Phys. D: Appl. Phys.* **48**(38), 385303 (2015).
42. N. Bidaraguppe Ramesh, F. Schmidt, and A. Schindlmayr, "Lattice parameters and electronic bandgap of orthorhombic potassium sodium niobate $\text{K}_{0.5}\text{Na}_{0.5}\text{NbO}_3$ from density-functional theory," *Eur. Phys. J. B* **94**(8), 169 (2021).
43. F. Schmidt, M. Landmann, E. Rauls, *et al.*, "Consistent Atomic Geometries and Electronic Structure of Five Phases of Potassium Niobate from Density-Functional Theory," *Adv. Mater. Sci. Eng.* **2017**, 1–13 (2017).
44. T. Murauskas, V. Kubilius, Z. Saltyte, *et al.*, "Metalorganic chemical vapor deposition and investigation of nonstoichiometry of undoped BaSnO_3 and La-doped BaSnO_3 thin films," *Thin Solid Films* **692**, 137575 (2019).
45. P. Li, S. Ouyang, G. Xi, *et al.*, "The Effects of Crystal Structure and Electronic Structure on Photocatalytic H_2 Evolution and CO_2 Reduction over Two Phases of Perovskite-Structured NaNbO_3 ," *J. Phys. Chem. C* **116**(14), 7621–7628 (2012).
46. Y. P. Varshni, "Temperature Dependence of The Energy Gap in Semiconductors," *Physica* **34**(1), 149–154 (1967).
47. M. DiDomenico and S. H. Wemple, "Oxygen-Octahedra Ferroelectrics. I. Theory of Electro-optical and Nonlinear optical Effects," *J. Appl. Phys.* **40**(2), 720–734 (1969).
48. A. Lynnyk, D. Chvostova, O. Pacheroova, *et al.*, "Optical properties of epitaxial relaxor ferroelectric $\text{PbSc}_{0.5}\text{Nb}_{0.5}\text{O}_3$ films," *Appl. Phys. Lett.* **103**(13), 132901 (2013).
49. P. Lautenschlager, M. Garriga, L. Vina, *et al.*, "Temperature dependence of the dielectric function and interband critical points in silicon," *Phys. Rev. B* **36**(9), 4821–4830 (1987).
50. S. Azam, M. Irfan, Z. Abbas, *et al.*, "Electronic structure and optical properties of cubic NaNbO_3 and tetragonal KNbO_3 crystals: first principles study," *Dig. J. Nanomater. Biostructures* **14**, 751–760 (2019).
51. T. D. Kang, H. Lee, G. Xing, *et al.*, "Dielectric functions and critical points of PbTiO_3 , PbZrO_3 , and $\text{PbZr}_{0.5}\text{Ti}_{0.43}\text{O}_3$ grown on SrTiO_3 substrate," *Appl. Phys. Lett.* **91**(2), 022918 (2007).
52. S. Azama, M. Irfan, Z. Abbas, *et al.*, "Electronic structure and optical properties of cubic NaNbO_3 and tetragonal KNbO_3 crystals: first principles study," *Dig. J. Nanomater. Biostructures* **14**, 751–760 (2019).
53. X. Chen, P. P. Jiang, Z. H. Duan, *et al.*, "The A-site driven phase transition procedure of $(\text{Pb}_{0.97}\text{La}_{0.02})(\text{Zr}_{0.42}\text{Sn}_{0.40}\text{Ti}_{0.18})\text{O}_3$ ceramics: An evidence from electronic structure variation," *Appl. Phys. Lett.* **103**(19), 192910 (2013).
54. Q. Li, J. Wang, M. Li, *et al.*, "Structure evolution mechanism of $\text{Na}_{0.5}\text{Bi}_{2.5}\text{Nb}_{2-x}\text{W}_x\text{O}_{9+\delta}$ ferroelectric ceramics: Temperature-dependent optical evidence and first-principles calculations," *Phys. Rev. B* **96**(2), 024101 (2017).
55. S. Simsek, H. Koc, V. A. Trepakov, *et al.*, "Electron Spectroscopy and the Electronic Structure of KNbO_3 : First Principle Calculations," *Ferroelectrics* **461**(1), 99–105 (2014).
56. T. Neumann, G. Borstel, C. Scharfschwerdt, *et al.*, "Electronic structure of KNbO_3 and KTaO_3 ," *Phys. Rev. B* **46**(17), 10623–10628 (1992).
57. T. P. Sinha, A. Dutta, S. Saha, *et al.*, "Electronic structure and optical properties of ordered compounds potassium tantalate and potassium niobate and their disordered alloys," *Phys. B (Amsterdam, Neth.)* **407**(24), 4615–4621 (2012).
58. M. Tyunina, L. D. Yao, D. Chvostova, *et al.*, "Effect of epitaxy on interband transitions in ferroelectric KNbO_3 ," *New J. Phys.* **17**(4), 043048 (2015).
59. M. Tyunina, D. Chvostova, L. D. Yao, *et al.*, "Interband transitions in epitaxial ferroelectric films of NaNbO_3 ," *Phys. Rev. B* **92**(10), 104101 (2015).
60. M. Tyunina, J. Narkilahti, J. Levoska, *et al.*, "Ultrathin SrTiO_3 films: epitaxy and optical properties," *J. Phys.: Condens. Matter* **21**(23), 232203 (2009).
61. K. Kang, S. Bin Anooz, J. Schwarzkopf, *et al.*, "Spontaneous polarization in NaNbO_3 film on NdGaO_3 and DyScO_3 substrates," [arxiv http://arxiv.org/abs/2311.13266](http://arxiv.org/abs/2311.13266) (2023).
62. R. V. Pisarev, A. S. Moskvina, A. M. Kalashnikova, *et al.*, "Charge transfer transitions in multiferroic BiFeO_3 and related ferrite insulators," *Phys. Rev. B* **79**(23), 235128 (2009).
63. J. Zhang, W.-Y. Tong, J. Zhu, *et al.*, "Temperature-dependent lattice dynamics and electronic transitions in $0.93\text{Pb}(\text{Zn}_{1/3}\text{Nb}_{2/3})\text{O}_3$ – 0.07PbTiO_3 single crystals: Experiment and theory," *Phys. Rev. B* **91**(8), 085201 (2015).